A light-triggered protein secretion system

Daniel Chen, Emily S. Gibson, and Matthew J. Kennedy

Department of Pharmacology, University of Colorado Denver School of Medicine, Aurora, CO 80045

ptical control of protein interactions has emerged as a powerful experimental paradigm for manipulating and studying various cellular processes. Tools are now available for controlling a number of cellular functions, but some fundamental processes, such as protein secretion, have been difficult to engineer using current optical tools. Here we use UVR8, a plant photoreceptor protein that forms photolabile homodimers, to engineer the first light-triggered protein secretion system. UVR8 fusion proteins were conditionally

sequestered in the endoplasmic reticulum, and a brief pulse of light triggered robust forward trafficking through the secretory pathway to the plasma membrane. UVR8 was not responsive to excitation light used to image cyan, green, or red fluorescent protein variants, allowing multicolor visualization of cellular markers and secreted protein cargo as it traverses the cellular secretory pathway. We implemented this novel tool in neurons to demonstrate restricted, local trafficking of secretory cargo near dendritic branch points.

Introduction

The use of light to control basic cellular functions has transformed experimental biology. Some of the first approaches relied on photolabile small molecule analogues of second messengers, second messenger chelators, or neurotransmitters to control cellular physiology and signaling pathways with ultraviolet (UV) light (Kaplan and Somlyo, 1989; Callaway and Katz, 1993; Ellis-Davies and Kaplan, 1994; Ellis-Davies, 2007). These "caged" compounds have been invaluable for dissecting numerous molecular pathways governing cellular physiology with unprecedented spatial and temporal control.

More recently, exogenously expressed photoreceptors from plants have been used to control cellular biochemistry by conditionally gating protein—protein interactions with light (Tucker, 2012). This approach has emerged as a new and powerful way to control cellular processes on fast timescales with fine spatial precision without the need for small molecules. Some of the first studies describing engineered optical control of cellular functions used the plant photoreceptor phytochromeB (PhyB; Shimizu-Sato et al., 2002; Tyszkiewicz and Muir, 2008; Levskaya et al., 2009). PhyB binds to members of the phytochrome-interacting family (PIF) of basic helix-loop-helix transcription factors when photoexcited with red (660 nm) light (Ni et al., 1998; Leivar et al., 2008). Remarkably, PhyB/PIF interactions can be reversed by near-infrared (730 nm) excitation, allowing fast and local toggling of PIF binding (Ni et al., 1999; Levskaya et al., 2009).

Correspondence to Matthew J. Kennedy: matthew.kennedy@ucdenver.edu Abbreviations used in this paper: FKBP, FK506-binding protein; mCh, monomeric cherry; UV, ultraviolet; UVR8, UV resistance locus8; VSVG, vesicular stomatitis virus glycoprotein.

However, PhyB-based systems require addition of an exogenous phycocyanobilin chromophore that is not normally present in yeast, flies, worms, or mammals, making it more difficult to implement than more recently developed systems that are entirely genetically encoded. These systems rely on blue light photoreceptor cryptochrome2 (Cry2), which binds to cryptochrome-interacting basic-helix-loop-helix 1 (CIB1) in response to blue light, and the light, oxygen, voltage (LOV) domain photoreceptors, which undergo a large conformational change when photoexcited (Harper et al., 2003, 2004; Liu et al., 2008; Strickland et al., 2008, 2012; Wu et al., 2009; Yazawa et al., 2009; Kennedy et al., 2010; Lungu et al., 2012).

These tools have proven to be extremely powerful for controlling a wide range of cellular processes, including cell migration/ morphology, cell cycle progression, transcription, and DNA recombination. However, some fundamental cellular processes, such as protein secretion, have been difficult to engineer for optical control using currently available tools. Traditional approaches for conditionally controlling protein secretion, including temperature-sensitive trafficking mutants and more recent chemical—genetic strategies have been indispensable for dissecting the mechanisms of mammalian secretory trafficking (Lodish and Weiss, 1979; Presley et al., 1997; Rivera et al., 2000; Boncompain et al., 2012). Although extremely powerful, these approaches require extended incubation at nonpermissive

© 2013 Chen et al. This article is distributed under the terms of an Attribution–Noncommercial–Share Alike–No Mirror Sites license for the first six months after the publication date [see http://www.rupress.org/terms]. After six months it is available under a Creative Commons License [Attribution–Noncommercial–Share Alike 3.0 Unported license, as described at http://creativecommons.org/licenses/by-nc-sa/3.0/).

Downloaded from http://rupress.org/jcb/article-pdf/201/4/631/1580010/jcb_201210119.pdf by guest on 03 December 2025

temperatures or addition of small molecules, which can be costly, can have potential off-target effects, lack spatial precision, and can complicate large-scale screening efforts. Thus, we sought to circumvent these issues by engineering a system for optical control of protein secretion to complement and extend the current secretory trafficking toolkit.

Here we implement UVR8, a recently described plant photoreceptor protein, as an optogenetic actuator module for protein secretion (Rizzini et al., 2011; Christie et al., 2012; Wu et al., 2012). UVR8 has many unique properties that lend itself to this application, including constitutive formation of photolabile homodimers, slow reversal kinetics, and a UV-B absorption profile, which enables multicolor imaging of all widely used fluorescent proteins without activating the photoreceptor. We show that UVR8 can be used to conditionally sequester secretory cargo in the ER and that light triggers robust forward trafficking to the plasma membrane. We use this novel tool in neurons, where we demonstrate spatially constrained forward trafficking of secretory cargo at dendritic branch points.

Results

Characterization of UVR8 as an optical tool in mammalian cells

Because UVR8 has not been characterized for use as an optical tool in live mammalian cells, we evaluated the efficiency of UVR8 dimerization and its excitation properties in HEK293T cells using a plasma membrane recruitment assay that has been described in previous studies (Fig. 1 A; Inoue et al., 2005; Levskaya et al., 2009; Yazawa et al., 2009; Kennedy et al., 2010). We expressed UVR8 fused to EGFP containing a C-terminal CaaX prenylation motif (memGFP), which localizes to the plasma membrane, along with UVR8 fused to mCherry (UVR8-mCh). UVR8-mCh is normally cytosolic, but when coexpressed with UVR8-memGFP, a large fraction of the protein is localized to the plasma membrane, even after the cells have been exposed to room light, or laser illumination at 405, 488, or 561 nm used to visualize CFP, GFP, and mCh (Fig. 1 B).

To test if excitation energy at shorter wavelengths could dissociate the UVR8 dimerization pair in a mammalian system, we exposed cells expressing UVR8-memGFP and UVR8-mCh to a brief (3 s) pulse of UV-B (0.3 mW/cm², 312-nm narrow band) illumination. Upon UV-B illumination, UVR8-mCh immediately began dissociating from the plasma membrane and accumulating in the cytosol (Fig. 1, B–D; Video 1). To determine the minimal amount of UV-B required for dissociation, we measured the baseline cytoplasmic level of UVR8-mCh and then exposed cells to UV-B for durations ranging from 0.5 to 10 s (Fig. 1, E and F). After the first UV-B pulse, we incubated cells in darkness for 10 s to allow UVR8-mCh to dissociate, and then delivered a second, saturating dose of light to assay how much UVR8-mCh still remained associated with the plasma membrane. We found that 7 s of illumination (0.3 mW/cm², 312-nm narrow band) was sufficient to translocate 90% of plasma membrane-bound UVR8-mCh to the cytosol, with 50% dissociation occurring after 2–3 s (Fig. 1 F).

To test if UVR8, once monomerized, would reassociate over time, we dissociated UVR8-mCh from the plasma membrane

with a 7-s UV-B exposure and then incubated the cells in the dark for varying times from 0.5 to 8 h. The cells were treated with 25 μ M cycloheximide during the dark incubation period to prevent new protein synthesis and apparent recovery of plasma membrane–bound UVR8-mCh due to newly synthesized UVR8-memGFP and UVR8-mCh. We found that UVR8-mCh did not appreciably redimerize with UVR8-memGFP over the time scale of the experiment (8 h; Fig. S1).

UV-B toxicity

A major concern is that UV treatment can cause serious damage to cells that can ultimately lead to cell death. Thus, it is important to assay toxicity at the levels of light required to dissociate UVR8 dimers. Although no immediate effects on cell morphology were observed in the minutes or hours after UV-B treatment, we determined long-term cell viability following UV-B treatments identical to those used in our plasma membrane dissociation studies (Fig. S2 A). We tested for UV-B toxicity in Cos7 cells, HEK293 cells, and primary cultures of hippocampal neurons treated with UV-B for varying durations and assayed for cell viability using two different standard assays: propidium iodide and annexin V staining (Fig. S2). For cells treated with 3 or 5 s of UV-B (illumination that triggers 55 and 70% dissociation, respectively), cell viability was identical to dark controls. We did observe limited toxicity in all cell types when we treated cells for longer durations. For example, COS7 cells exposed to UV-B for 7 and 10 s (illumination that triggers \sim 90 and 99% dissociation, respectively) caused a 12 \pm 9% and $16 \pm 7\%$ loss in cell viability, respectively (Fig. S2 A). However, neurons and HEK293 cells were more resistant to these UV-B doses (Fig. S2, C and D). It is of note that UVR8 has also been used in yeast two-hybrid assays, indicating that levels of UV-B required for UVR8 dissociation were also minimally toxic to yeast (Rizzini et al., 2011).

As a potential alternative to UV-B excitation, we also tested whether UVR8 could be dissociated with two-photon (2-p) illumination using a femtosecond pulsed laser source (Chameleon Ultra II; Coherent Inc.) tuned to the shortest wavelength possible (690 nm). This would offer many advantages over single photon excitation including better tissue penetration, less potential for toxicity, and a more precise focal excitation volume. However, 690-nm excitation failed to appreciably monomerize UVR8 at a range of laser intensities or pixel dwell times (Fig. S3). It may be possible that 2-p excitation at shorter wavelengths (~600 nm) will trigger dissociation of UVR8 dimers, but this will require the use of more sophisticated optical hardware such as optical parametric oscillators to generate shorter wavelength pulsed excitation energy.

Optical control of protein secretion

The ability to conditionally trigger protein trafficking through the cellular secretory pathway with light would be an extremely powerful experimental tool, but currently there are no available methods to accomplish this. Previous approaches have relied on either temperature-sensitive mutants of secreted proteins (Lodish and Weiss, 1979; Presley et al., 1997) or chemical—genetic strategies that use small molecules to release proteins sequestered

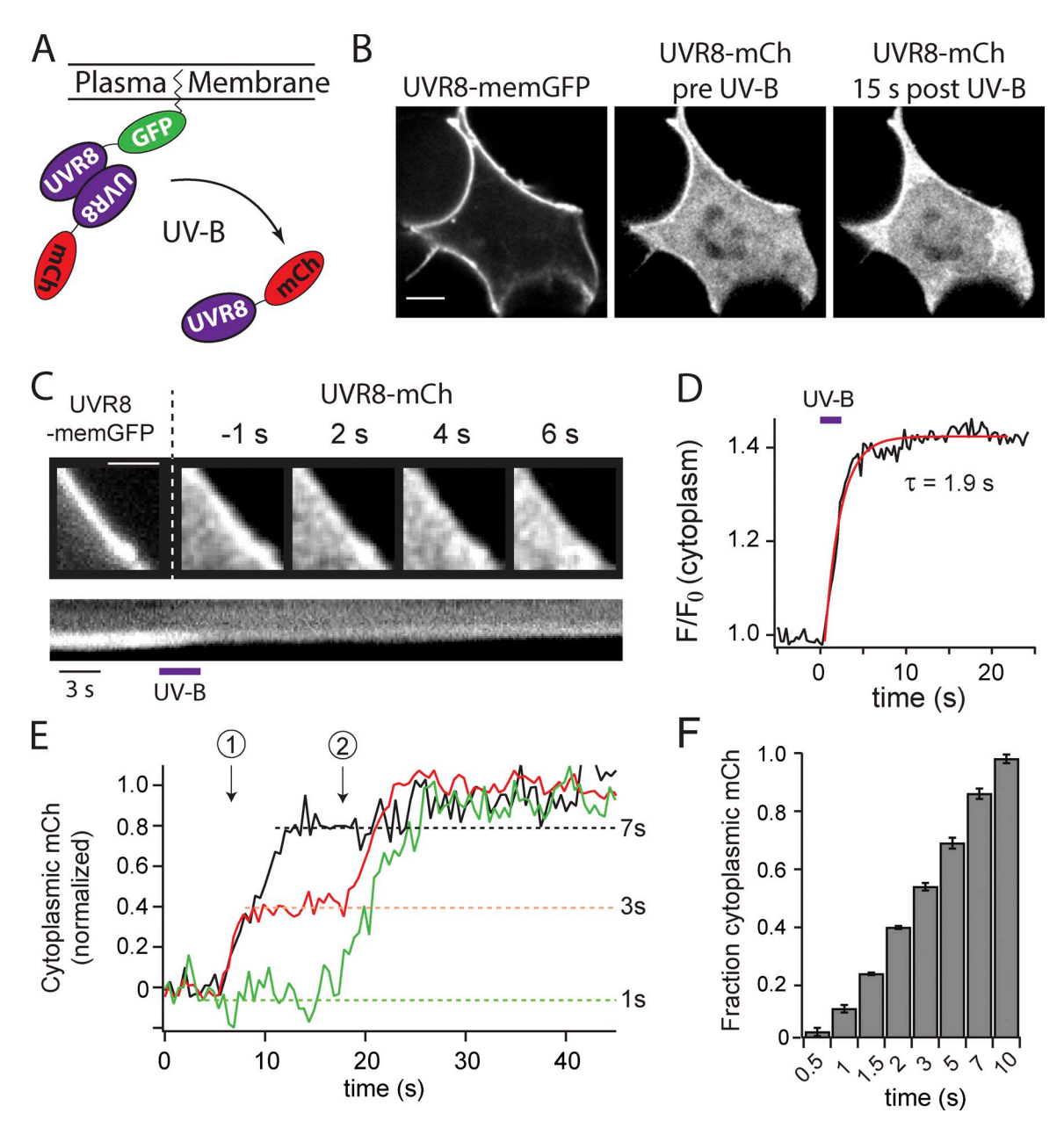


Figure 1. **Light-triggered dissociation of UVR8-tagged proteins.** (A) Schematic of light-triggered dissociation experiment. UVR8 fused to prenylated GFP (UVR8-memGFP) localizes to the plasma membrane where it recruits UVR8-mCh. Dissociation of the UVR8 dimer releases UVR8-mCh to the cytosol. (B) A HEK293T cell expressing UVR8-memGFP along with UVR8-mCh. Note the strong plasma membrane association of both GFP and mCh signals before UV-B illumination. mCh signal is mostly cytosolic 15 s after a brief (3 s) exposure to UV-B. Bar, 5 μm. (C) Time course of UVR8-mCh dissociation from the plasma membrane. Left-most panel shows the UVR8-memGFP localization at the plasma membrane. After UV-B treatment, the mCh signal rapidly dissociates from the plasma membrane. Bar, 1.5 μm. The kymograph shows the complete time course of translocation after a 3-s UV-B treatment (purple bar). Bar, 1 μm. (D) Cytosolic mCh signal was quantified and fit with a single exponential equation. The average time constant (τ) for UVR8 dissociation was 1.9 ± 0.2 s (n = 4 cells from 2 independent experiments). (E) Cytosolic mCh signal was quantified after varying durations of UV-B (arrow 1), followed by a saturating (10 s) UV-B exposure (arrow 2) to determine the fraction of UV-B remaining on the plasma membrane. Shown is representative data from single trials (with each exposure duration performed on a different cell on a fresh coverslip). (F) Average results of the light titration experiment shown in E. At least four different cells were quantified for each condition from four separate experiments. Error bars represent standard deviations of the mean.

in the ER (Rivera et al., 2000; Jaiswal et al., 2009; Al-Bassam et al., 2012; Boncompain et al., 2012). We based our strategy on a previously developed chemical–genetic strategy that uses an FK506-binding protein mutant (FKBP_{F36M}) that forms homodimers that can be dissociated with the rapamycin derivative AP21998 (Rollins et al., 2000). In this system, tandem copies of FKBP_{F36M} are fused to a secreted protein, which promotes the formation of high-order oligomers that are efficiently

trapped in the ER. Disrupting these oligomers with AP21998 allows forward trafficking from the ER to the Golgi apparatus and ultimately to the plasma membrane (Rivera et al., 2000). Given its slow reversibility, fast dissociation kinetics, and UV excitation profile, we reasoned that UVR8 would be the ideal photoreceptor module to engineer a similar system that uses light instead of a small molecule to trigger synchronous secretory trafficking.

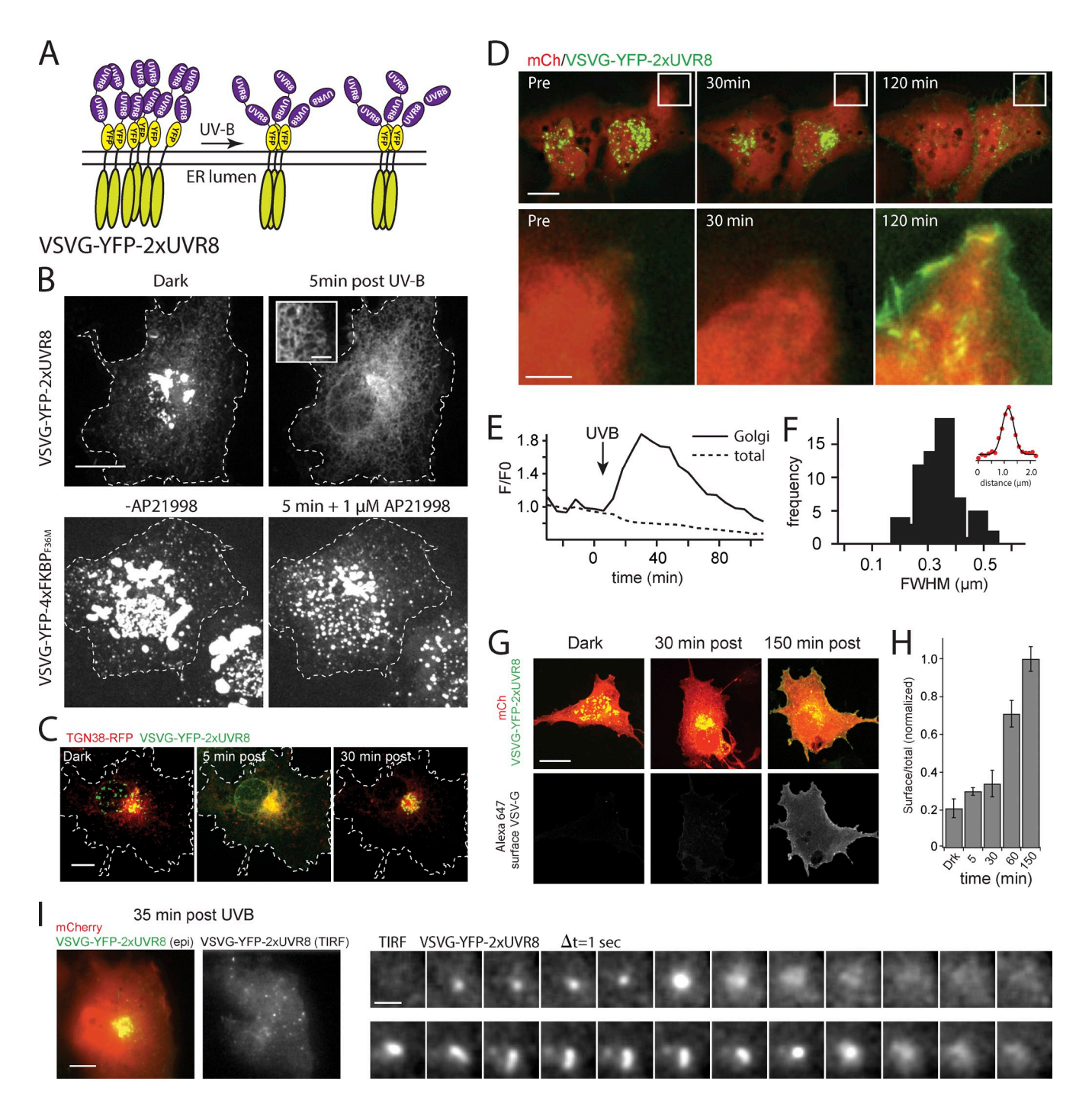


Figure 2. Light-triggered protein secretion. (A) Schematic for UVR8-dependent ER retention. Tandem copies of UVR8 fused to VSVG results in oligomers that are retained in the ER. Exposure to UV-B triggers dissociation of these clusters, allowing forward trafficking through the secretory pathway. (B) Comparison of light- and chemical-mediated ER release. VSVG-YFP-2×UVR8 (top panels) and VSVG-4×FKBP_{F36M} (bottom panels) were expressed in COS7 cells. Note the similar clustered appearance of both fusion proteins in the left panels. The right panels show the distribution of fusion proteins 5 min after UV-B exposure (top right) or addition of 1 µM AP21998 (bottom right). Note that UV-B treatment completely dissociates VSVG clusters, revealing the reticular structure of the ER (inset, top right), but AP21988 did not completely dissociate VSVG-4×FKBP_{F36M} clusters. Bar, 10 µm (inset, 2.5 µm). (C) Trafficking of VSVG-YFP-2×UVR8 (green) from ER to Golgi membranes labeled with TGN38-RFP (red). VSVG-YFP-2×UVR8 was nearly completely localized to the Golgi 30 min after UV-B treatment. Bar, 10 µm. (D) Trafficking of UVR8 to the plasma membrane after UV-B treatment. Cos7 cells expressing mCh (red) and VSVG-YFP-2×UVR8 (green) were treated with UV-B for 7 s and imaged periodically over the course of 2 h. The bottom panels show the periphery of the cell with the green channel adjusted so that the plasma membrane signal is visible. Bars: (top panels) 10 µm; (bottom panels) 2.5 µm. (E) Kinetics of Golgi complex accumulation and release after UV-B treatment. Shown is a representative example from one cell out of ten cells imaged from five independent experiments. (F) Distribution of sizes of post-Golgi carriers. Full width at half maximal (FWHM) values for mobile post-Golgi carriers were determined by a Gaussian fit of line scans across the carriers (see Video 4). The inset shows a representative Gaussian fit (black line) to the line scan data (red circles). 93 carriers were quantified from 3 different cells from a single experiment. (G) Cells expressing mCh (red) and VSVG-YFP-2xUVR8 (green, top panels) were surface labeled with anti-VSVG at various times after UV-B treatment (bottom panels). Bar, 10 µm. (H) Quantification of the surface label at different time points is shown in the bar graph to the right. Data are expressed as a normalized ratio of surface (anti-VSVG) signal to the total YFP signal. Error bars represent the standard deviation of the

To test if UVR8 could be implemented as a photoswitch for secretory trafficking, we fused one, two, or three copies of UVR8 to the C-terminal intracellular domain of vesicular stomatitis virus glycoprotein (VSVG) tagged with YFP (Fig. 2 A; Fig. S4). VSVG was chosen because its trafficking properties are well documented (Nishimura and Balch, 1997; Presley et al., 1997; Cole et al., 1998; Toomre et al., 2000; Schmoranzer and Simon, 2003). As expected, we observed large clusters of YFP signal in the ER of cells expressing VSVG-YFP fused to multiple (2x or 3x) copies of UVR8, which were very similar in size and distribution to VSVG-YFP-4×FKBP_{F36M} (Fig. 2 B; Fig. S4 A). A brief (7 s) exposure to UV-B triggered massive redistribution of the YFP signal, which quickly diffused throughout the ER (Fig. 2 B; Videos 2 and 3). We compared VSVG-YFP-2×UVR8 with VSVG-YFP-4×FKBP_{F36M} and found that whereas a brief pulse (7 s) of UV-B completely dissolved VSVG-YFP-2×UVR8 clusters within 5 min, 1 µM AP21998 treatment incompletely disrupted VSVG-YFP-4×FKBP_{F36M} clusters 5 min after application (Fig. 2 B). Imaging for longer time periods demonstrated that VSVG-YFP-2×UVR8 efficiently trafficked to the Golgi apparatus within 30 min, similar to previous reports using either temperature-sensitive VSVG mutants or chemical-genetic strategies to release VSVG from the ER (Fig. 2 C; Hirschberg et al., 1998; Toomre et al., 2000; Schmoranzer and Simon, 2003; Jaiswal et al., 2009). After 120 min, cells displayed robust surface expression of VSVG-YFP-2×UVR8 and nearly complete "emptying" of the Golgi complex (Fig. 2, D and E). We estimated that $95 \pm 2\%$ of ER-retained VSVG-YFP-2×UVR8 is trafficked to the plasma membrane 2.5 h after UV-B treatment. Disappearance of signal from the Golgi complex was accompanied by formation of mobile post-Golgi carriers (Video 4). The size of these carriers was determined by a Gaussian fit of pixel intensities along a line drawn through the widest aspect of the vesicle. The full width at half maximal (FWHM) sizes ranged from ~200 nm (near the diffraction limit of light) to \sim 600 nm (Fig. 2 F), similar to a previous study (Hirschberg et al., 1998). Insertion of VSVG-YFP-2×UVR8 into the plasma membrane was confirmed by staining with an antibody that recognizes an extracellular VSVG epitope at various times after UV-B exposure and revealed a 5-10-fold increase in surface VSVG 150 min after UV-B treatment (Fig. 2, G and H). As an independent verification of trafficking to the plasma membrane, we performed total internal reflection fluorescence (TIRF) microscopy to directly visualize post-Golgi carriers fusing with the plasma membrane (Fig. 2 I; Videos 5 and 6). Cos7 cells were imaged in TIR mode 35-40 min after UV-B treatment to allow time for cargo to accumulate in post-Golgi carriers destined for the plasma membrane. Fig. 2 I and Videos 5 and 6 show mobile post-Golgi carriers fusing with the plasma membrane in UV-B-treated cells. We never observed fusion events in cells not treated with UV-B. Fusion events in

UV-B-treated cells were consistent with previous studies using TIRF microscopy to observe VSVG plasma membrane insertion (Schmoranzer et al., 2000; Toomre et al., 2000).

Optical control of protein trafficking in neurons

Neurons are the largest and most morphologically complex cells in the body, with membrane surface areas ~10,000 times that of typical epithelial cells (Horton and Ehlers, 2003b). Their immense size, polarity, and architectural complexity place extraordinary demands on the neuronal secretory pathway. However, it has been difficult to study the neuronal secretory pathway with traditional tools. For example, primary neuronal cultures respond poorly to the extended 40°C incubation required for ER accumulation of the temperature-sensitive ts045 variant of VSVG. Other methods hold promise, but require addition of expensive chemical ligands (Rivera et al., 2000; Al-Bassam et al., 2012) or specially formulated media lacking biotin, which is included in commercial neuronal media supplements (Boncompain et al., 2012). Our system overcomes these issues by circumventing the requirement for added chemicals or elevated temperatures.

Expression of VSVG-YFP-UVR8 in neurons resulted in the expected punctate expression pattern in the soma, but we also observed clusters throughout neuronal dendritic arbors due to the continuity of ER throughout the somatodendritic compartment (Fig. 3 A). Exposure of neurons to UV-B illumination dissolved these clusters and resulted in a uniform localization that extended throughout the soma and dendrites 5 min after UV-B treatment (Fig. 3 B). After 30 min, we observed that most VSVG-YFP-2×UVR8 signal had redistributed to perinuclear Golgi membranes in the soma (Fig. 3, A and B). We confirmed that VSVG-YFP-2×UVR8 ultimately accumulated at the neuronal plasma membrane by surface labeling neurons with an antibody against an extracellular VSVG epitope at various times after UV-B treatment (Fig. 3, B and C). In neurons we observed an ~30-fold increase in VSVG surface label 150 min after UV-B.

Local trafficking in neuronal dendrites

After UV-B treatment, we often observed accumulation of VSVG cargo at dendritic branch points (Fig. 3 D; Video 7). These branch point clusters have been previously described as dendritic "Golgi outposts," and are thought to represent platforms for local trafficking of dendritic secretory cargo (Horton and Ehlers, 2003a; Horton et al., 2005). However, given the somatodendritic continuity of ER, it is impossible to know whether accumulated cargo at branch point Golgi membranes originates from branch point ER (locally), or whether it is trafficked to branch points from distal sites, such as somatic ER. We thought this an important distinction because synaptic activity drives local protein synthesis in dendrites, which leads to incorporation of important neuronal proteins in the dendritic plasma membrane. Indeed,

mean from three different experiments. At least four cells were measured for each time point. (I) TIRF microscopy visualizing fusion of post-Golgi carriers with the plasma membrane. A wide-field fluorescent image of a COS7 cell expressing mCherry (red) and VSVG-YFP-3×UVR8 (green) is shown in the left panel and the TIRFM image of the same cell is in the middle panel. Bar, 10 µm. The image sequence to the right shows TIRFM imaging of post-Golgi carriers fusing with the plasma membrane. Bar, 1 µm.

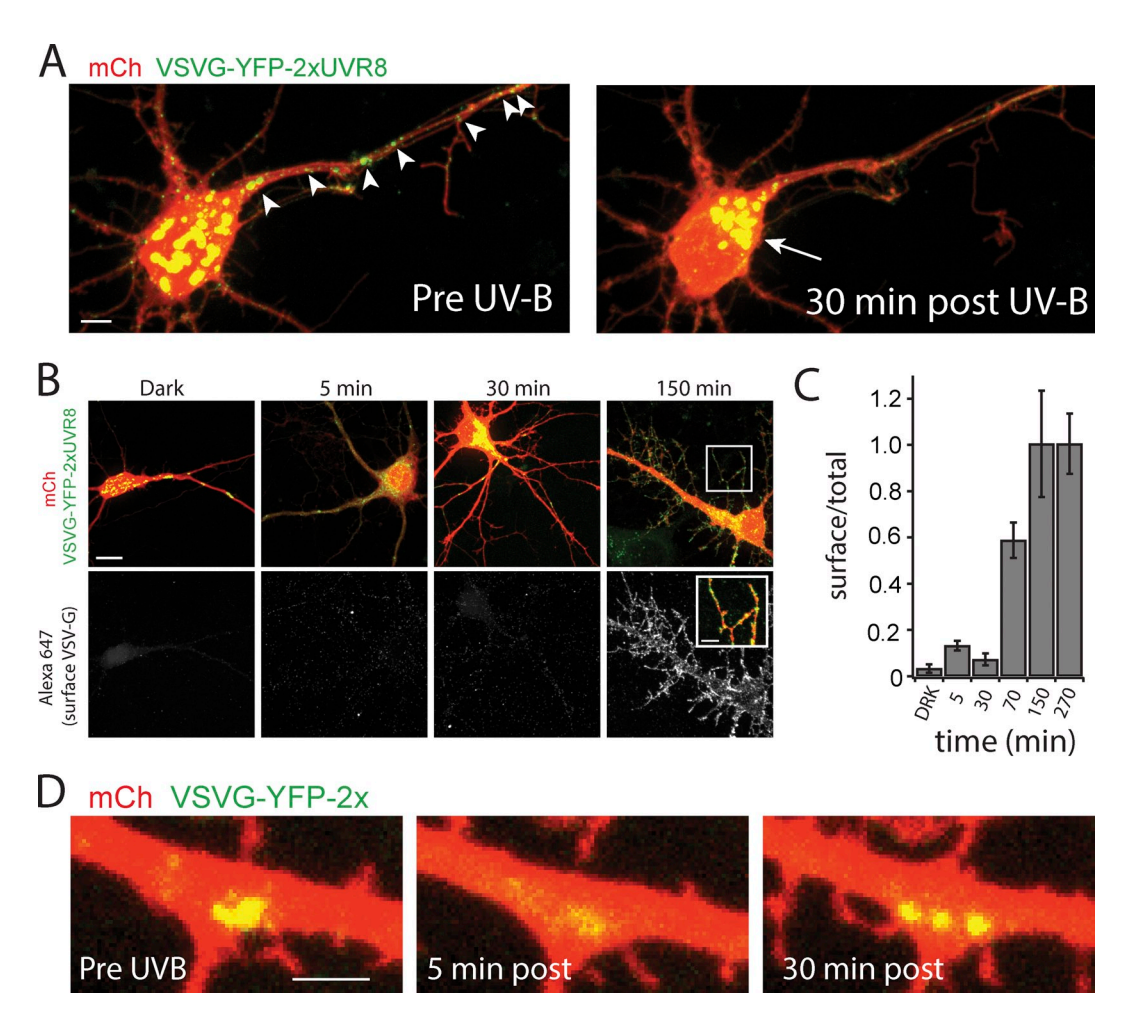


Figure 3. **Light-triggered protein secretion in neurons.** (A) Localization of VSVG-2xUVR8 in neurons before UV-B treatment. Note the localization of clusters in the soma and in dendritic processes (arrowheads). The same cell was imaged 30 min after UV-B treatment (right). Note the massive redistribution of signal to the somatic Golgi (arrow). Bar, 4 μ m. (B) Hippocampal neurons expressing VSVG-YFP-2xUVR8 (green) and mCherry (red) were labeled with an antibody against an extracellular epitope of VSVG (bottom panels) at various times after UV-B treatment. In the dark, VSVG surface labeling was not significantly greater than background values, but robustly increased after UV-B treatment. The inset in the bottom right panel shows VSVG surface label (green) overlaid with mCh cell fill (red). Bar, 10 μ m (inset, 4 μ m). (C) Quantification of data from B. 150 min after UV-B treatment, we observed a >30-fold increase in VSVG surface expression. Data are expressed as a normalized ratio of surface (anti-VSVG) signal to the total YFP signal (n = at least 4 cells for each time point). Error bars represent the standard deviation of the mean. (D) Formation of dendritic trafficking outposts. VSVG-YFP-2xUVR8 clusters were dissolved with UV-B (middle); we often observed a delayed accumulation of cargo in Golgi outposts positioned near dendritic branch points (right). Bar, 2 μ m.

local protein synthesis in dendrites is thought to be critical for important forms of plasticity, but if newly synthesized secreted proteins quickly diffused away from sites of synthesis (in the ER membrane) before they could be captured for forward trafficking, any activity-induced spatial enrichment of newly synthesized proteins would be lost. A recent study demonstrated that the morphological complexity of the ER near dendritic branch points can act as a diffusion trap, presumably to restrict diffusion of ER proteins and to limit forward trafficking to nearby Golgi membranes (Cui-Wang et al., 2012).

To directly test whether ER-to-Golgi secretory trafficking could be spatially restricted in dendrites, we fused VSVG-2×UVR8 to the photoswitchable protein mEOS2 (Zhang et al., 2012), which can be photoconverted from green to red with 405-nm excitation (Fig. S5; Fig. 4 A). This allows us to locally "tag" ER-retained secretory cargo in different subcellular domains (e.g., dendrites, branch points, or soma) with focal 405-nm excitation before ER release with UV-B (Fig. 4 B). We first

confirmed that photoswitching with focal 405-nm illumination did not itself trigger UVR8 dissociation (Fig. 4 A). After 405-nm photoconversion, VSVG-mEOS2-2×UVR8 clusters remained intact, indicating that UVR8 was not sensitive to focal photoswitching illumination. Conversely, we also confirmed that global UV-B illumination used to dissociate UVR8 does not also photoconvert mEOS from green to red, as this would complicate tracking locally photoswitched secretory cargo. After UV-B treatment, we observed rapid dissociation of VSVG-mEOS2-2×UVR8 clusters, but no increase in overall red signal, confirming that UV-B does not trigger mEOS2 photoswitching; however, we did observe limited photoactivation of the green form of mEOS2 with UV-B (Fig. 4 A; Fig. S5).

Dendritic branch points have been implicated as trafficking "hot spots" for newly synthesized proteins based on the prevalence of ribosomes, secretory organelles, and high ER surface area/morphological complexity at branch points compared with surrounding dendritic regions (Horton et al., 2005; Cui-Wang

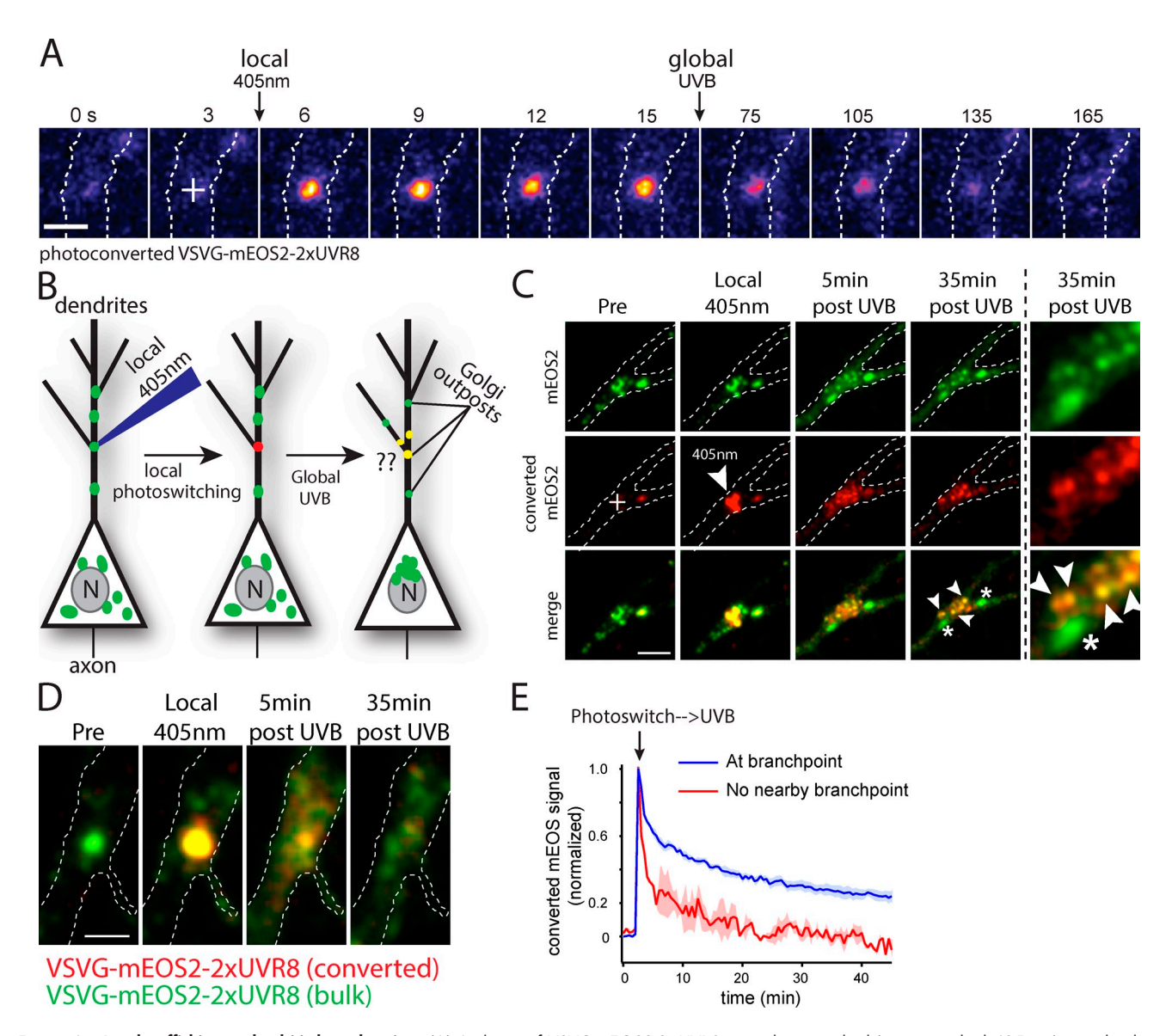


Figure 4. Local trafficking at dendritic branch points. (A) A cluster of VSVG-mEOS2-2×UVR8 was photoswitched (arrow marked 405 nm) in a dendrite before global UV-B treatment (arrow marked UV-B) to release labeled cargo from the ER. Note that VSVG-mEOS2-2×UVR8 clusters remain intact after focal 405-nm illumination and can be subsequently dissolved with UV-B. Bar, 1 µm. (B) Experimental strategy. Branch point cargo can be selectively tagged and tracked by photoconverting mEOS-tagged VSVG-2×UVR8 before ER release with UV-B. (C) Branch point cargo was selectively photoconverted to red with local 405-nm illumination (crosshair, middle) and then released with global UV-B. Note the accumulation of red puncta at sites near the branch point after UV-B treatment (arrowheads). Not all nearby puncta contained photoswitched cargo (asterisks), indicating selective trafficking to a subset of branch point organelles. Bar, 4 µm. (D) Tracking non-branch point ER cargo. No local accumulation of secretory cargo was observed when we tagged ER cargo at sites distant from branch points. Bar, 3 µm. (E) Quantification of local photoswitching branch points vs. non-branch point ER before release. Branch point cargo was redistributed, but effectively retained for tens of minutes near its origin while non-branch point cargo quickly diffused away and diluted into the bulk, nonphotoconverted VSVG. n = at least 3 branch points and 5 different non-branch point sites from 3 different neurons. Data collected from three independent experiments. The shaded regions in the traces indicate the range of standard error of the mean.

et al., 2012). However, no study has directly addressed whether ER cargo originating near branch points is trafficked to nearby Golgi with any preference over cargo originating at distant sites. To address this issue, we locally photoconverted small regions (~1 µm in diameter) of ER-retained VSVG-mEOS2-2×UVR8 at dendritic branch points, or at dendritic sites >5 µm from branch points, and analyzed subsequent trafficking behavior after ER release (Fig. 4, B–E; Video 8). A significant fraction of cargo released from branch points redistributed to nearby Golgi membranes over the course of 35 min (Fig. 4 C; Video 8). Accumulation in Golgi outposts occurred with kinetics nearly identical

to the redistribution of cargo to the somatic Golgi, indicating no major differences in the rates of secretion for dendritic versus somatic proteins. This experiment demonstrates that forward trafficking from ER to Golgi membranes can occur for a significant fraction of cargo before it diffuses away from branch points in the ER membrane. We also tracked VSVG-mEOS2-2×UVR8 released from dendritic sites >5 μm from branch points. Little or no local redistribution/accumulation of VSVG was observed (Fig. 4, D and E). Thus, dendritic branch points selectively retain a significant fraction of cargo released from nearby ER, further supporting a model for restricted local secretory trafficking at

dendritic branch points. In these experiments we used VSVG, a nonneuronal cargo molecule, to investigate spatial determinants of neuronal protein secretion. Future experiments will test whether specific neuronal receptors are more or less efficiently trapped and trafficked at branch points as a mechanism for spatially controlling the composition of cell surface receptors at nearby dendritic branches and synapses.

Discussion

Here we developed a novel optogenetic tool for light-triggered control of protein secretion in mammalian cells. We selected the plant photoreceptor UVR8 for this application because it has distinct properties that favor it over currently available optogenetic tools: It can be used in conjunction with all popular fluorescent and photoswitchable proteins, operates on a fundamentally different principle than existing tools (protein dissociation rather than association), and once photoactivated is essentially irreversible for hours.

As a first demonstration of the utility of this approach, we tracked secretory cargo originating in dendritic branches to determine whether dendritic ER proteins undergo local secretory trafficking. Our data suggest that cargo released from the ER near branch points can be locally trafficked to dendritic Golgi membranes at branch points. Further experiments using fluorescent reporters for cargo delivery to the cell surface (e.g., superecliptic phluorin) will determine whether subsequent post-Golgi trafficking is also locally restricted. In these experiments we used VSVG, a nonneuronal cargo molecule, to investigate the spatial determinants of neuronal protein secretion. Future experiments will test whether specific neuronal receptors, cell adhesion molecules, or ion channels are more or less efficiently trapped and trafficked at branch points as a mechanism for spatially controlling the molecular composition and fundamental properties of nearby dendrites and whether synaptic activity influences this process.

In addition to studying the secretory system in morphologically complex cells such as neurons, we anticipate that this approach will be broadly adopted in multiple fields. For example, we see great potential for its use in screening for proteins or drugs influencing secretory trafficking, or for conditional and local release of morphogens or growth factors from light-targeted cell populations in developing embryos. UVR8-based tools will expand and complement existing systems by offering a new spectral channel for protein control and unique properties that will enable optical manipulation of a new set of cellular processes.

Materials and methods

Constructs

UVR8 cDNA was obtained from the TAIR consortium for Arabidopsis. UVR8-memGFP and UVR8-mCh were generated by PCR amplifying UVR8 and cloning into GFP-CaaX (Kennedy et al., 2010) or mCherry vectors. All VSVG-YFP-UVR8 clones were generated by PCR amplifying UVR8 and using standard cloning techniques to generate the 1x, 2x, and 3x versions. mEOS2 was obtained from Addgene. VSVG-mEOS2-2xUVR8 was generated by exchanging YFP for mEOS2 using the VSVG-YFP-2xUVR8 construct. All constructs used CMV promoter to drive expression. TGN38 was a kind gift from K. Howell (University of Colorado School of Medicine, Aurora, CO).

Cell culture and transfection

HEK293T and COS7 cells were maintained in DMEM with 10% FBS. Cells were transfected using Lipofectamine 2000 according to the manufacturer's instructions (Invitrogen). Cells were imaged 12–16 h after transfection. Longer transfection times and high expression levels led to higher basal levels (~30% of total) of VSVG-YFP-2×/3×-UVR8 at the plasma membrane; thus, we confined our experiments to 12–16 h after transfection.

Primary hippocampal neurons were prepared from neonatal Sprague-Dawley rats. Hippocampi were dissected from the brains of postnatal day 0–2 rats and dissociated by papain digestion. Neurons were plated at 60,000–70,000 cells/ml in MEM, 10% FBS (Hyclone) containing penicil-lin/streptomycin on poly-D-lysine-coated glass coverslips. After 1 d the media was replaced with Neurobasal-A supplemented with B27 (Invitrogen). The neurons were then fed with Neurobasal-A, B27, and mitotic inhibitors (uridine + fluoro-deoxyuridine [Ur+FdUr]) by replacing half the media on day 4 or day 5 and then twice weekly. For Lipofectamine 2000 transfections, neurons were transfected on DIV 5–6 with 1 µg of plasmid/1 µl of Lipofectamine according to the manufacturer's protocol and imaged on DIV 6–7. All animal procedures were performed in accordance with the University of Colorado School of Medicine guidelines.

Imagino

Live-cell imaging was performed at 32°C on a microscope (model IX71; Olympus) equipped with a spinning disc scan head (Yokogawa Corporation of America) with a 60×/NA 1.4 objective. Excitation illumination was delivered from an AOTF controlled laser launch (Andor Technology) and images were collected on a 1024 x 1024 pixel EM-CCD camera (iXon; Andor Technology). Data acquisition and analysis were performed with MetaMorph (Molecular Devices) and ImageJ (National Institutes of Health). Some images were smoothed (averaging over 3 × 3 pixels) using ImageJ for display, but never before quantification. COS7 or HEK293T cells were plated on 18-mm coverslips and imaged in a buffer containing the following (mM): 10 Hepes, 10 p-glucose, 140 NaCl, 3 KCl, 1 MgCl₂, and 1 CaCl₂. To trigger forward trafficking of ER-retained VSVG, cells were treated with diffuse illumination from a UV-B (312 nm) source (model EB280C; Spectroline) positioned 7 cm above the sample for 7–10 s. The intensity of light at the sample was measured at 0.3 mW/cm² For light titration experiments, the UV-B excitation was shuttered with a Uniblitz shutter controlled with a Master-8 stimulator (A.M.P.I.). For local photoactivation of mEOS2, 405-nm laser illumination was steered using galvometric laser-scanning mirrors (FRAPPA; Andor Technology). Two-photon excitation was performed on a microscope (model LSM510; Carl Zeiss) equipped with a laser (Chameleon Ultra II; Coherent Inc.) tuned to 690 nm and 50-65% of maximum power with 250-usec pixel dwell times. Higher excitation energy or slower pixel dwell times caused immediate membrane blebbing and cell death likely due to sample heating.

The size of post-Golgi carriers was determined by fitting the pixel intensities of a line drawn across the widest aspect of the vesicle with a Gaussian fit using Igor Pro software (Wavemetrics). The full width at half maximal value for post-Golgi carriers was extracted from the fits.

TIRF microscopy was performed on a microscope (model IX81; Olympus) equipped with a 10-mW argon laser fiber-coupled to a manual TIRFM illuminator. The temperature of the cells was controlled at 32°C. Images were recorded at 2 Hz on a CCD camera (Orca ER; Hamamatsu Photonics) using Slidebook software.

Immunocytochemistry

Surface VSVG was labeled with an antibody that recognizes an extracellular epitope (clone 8G5F11; Kerafast). After UV-B exposure, cells were incubated for various times before fixation for 10 min with 4% paraformaldehyde in PBS. Cells were washed in PBS and incubated with anti-VSVG overnight at a dilution of 1:1,000 in PBS with 5% BSA. Cells were washed and incubated with anti-mouse secondary antibody conjugated to Alexa Fluor 647.

UV-B toxicity

Primary hippocampal neurons, HEK293 cells, or COS7 cells were exposed to varying durations of UV-B illumination (312 nm, 0.3 mW/cm²) from a distance of 7 cm. For primary cultures of hippocampal neurons, 100 mM glutamate was added to the media as a positive control for neuronal cell death. 10% methanol was used as a positive control for COS7 and HEK293 cells. A nontreated negative control was included. After UV treatment and a subsequent 14-h incubation period in the dark, COS7 cells were resuspended in PBS and incubated in the dark with 2 µg/ml propidium iodide (Sigma-Aldrich) or annexin V Alexa Fluor 488 conjugate (5%; Invitrogen). Cells were then transferred to a microscope slide and coverslipped. Neurons were not resuspended before labeling. The number of live cells versus

dead cells was determined using a cell counter on a fluorescence microscope with excitation at 488 nm and emission at 516 nm for annexin V, and excitation at 516 nm and emission at 610 nm for propidium iodide.

UVR8 reversibility

HEK293 cells expressing UVR8-mCh and UVR8-memGFP were exposed to 7 s of UV-B light (312 nm, 0.3 mW/cm²) from a distance of 7 cm and then incubated for 2, 4, 6, and 8 h in the dark. Samples were treated with 25 μ M cycloheximide to prevent new protein synthesis. After dark incubation, samples were fixed for 10 min with 4% paraformaldehyde, washed, and mounted using Prolong Gold (Invitrogen). Confocal microscopy was performed to determine UVR8-mCh membrane localization.

Online supplemental material

Fig. S1 demonstrates a lack of reversibility of UVR8 dissociation. Fig. S2 shows UVB toxicity. Fig. S3 shows that UVR8 cannot be monomerized with conventional two-photon excitation at 690 nm. Fig. S4 compares ER retention of VSVG fused to 1, 2, or 3 copies of UVR8. Fig. S5 shows that UVR8 can be used with the photoswitchable protein mEOS2. Video 1 shows the dissociation kinetics of UVR8 in response to UVB excitation. Video 2 demonstrates light-triggered dissociation of ER-retained VSVG-YFP-2×UVR8 clusters. Video 3 shows light-triggered VSVG-YFP-2×UVR8 trafficking from ER to Golgi membranes. Video 4 shows the formation and mobility of VSVG-YFP-2×UVR8 post-Golgi carriers. Video 5 shows TIRFM imaging of post-Golgi carriers. Video 6 shows TIRFM imaging of post-Golgi carriers fusing with the plasma membrane. Video 7 shows trafficking of VSVG-YFP-2×UVR8 at dendritic branch points. Video 8 shows local photoconversion and release of VSVG-mEOS2-2×UVR8 at branch point and non-branch point dendritic regions. Online supplemental material is available at http:// www.jcb.org/cgi/content/full/jcb.201210119/DC1.

We would like to thank Chandra Tucker for critical discussions, Radu Moldovan and Greg Glazner of the Advanced Light Microscopy Core Facility at the University of Colorado School of Medicine, and Kathryn Howell and John Caldwell for providing constructs.

This work was supported by grants from the Brain and Behavior Research Foundation (M.J. Kennedy) and the Boettcher Foundation (M.J. Kennedy).

Submitted: 24 October 2012 Accepted: 11 April 2013

References

- Al-Bassam, S., M. Xu, T.J. Wandless, and D.B. Arnold. 2012. Differential trafficking of transport vesicles contributes to the localization of dendritic proteins. Cell Rep. 2:89–100. http://dx.doi.org/10.1016/j.celrep. 2012.05.018
- Boncompain, G., S. Divoux, N. Gareil, H. de Forges, A. Lescure, L. Latreche, V. Mercanti, F. Jollivet, G. Raposo, and F. Perez. 2012. Synchronization of secretory protein traffic in populations of cells. *Nat. Methods*. 9:493–498. http://dx.doi.org/10.1038/nmeth.1928
- Callaway, E.M., and L.C. Katz. 1993. Photostimulation using caged glutamate reveals functional circuitry in living brain slices. *Proc. Natl. Acad. Sci. USA*. 90:7661–7665. http://dx.doi.org/10.1073/pnas.90.16.7661
- Christie, J.M., A.S. Arvai, K.J. Baxter, M. Heilmann, A.J. Pratt, A. O'Hara, S.M. Kelly, M. Hothorn, B.O. Smith, K. Hitomi, et al. 2012. Plant UVR8 photoreceptor senses UV-B by tryptophan-mediated disruption of cross-dimer salt bridges. *Science*. 335:1492–1496. http://dx.doi.org/10.1126/science.1218091
- Cole, N.B., J. Ellenberg, J. Song, D. DiEuliis, and J. Lippincott-Schwartz. 1998. Retrograde transport of Golgi-localized proteins to the ER. *J. Cell Biol.* 140:1–15. http://dx.doi.org/10.1083/jcb.140.1.1
- Cui-Wang, T., C. Hanus, T. Cui, T. Helton, J. Bourne, D. Watson, K.M. Harris, and M.D. Ehlers. 2012. Local zones of endoplasmic reticulum complexity confine cargo in neuronal dendrites. *Cell*. 148:309–321. http://dx.doi.org/10.1016/j.cell.2011.11.056
- Ellis-Davies, G.C. 2007. Caged compounds: photorelease technology for control of cellular chemistry and physiology. *Nat. Methods.* 4:619–628. http://dx.doi.org/10.1038/nmeth1072
- Ellis-Davies, G.C., and J.H. Kaplan. 1994. Nitrophenyl-EGTA, a photolabile chelator that selectively binds Ca2+ with high affinity and releases it rapidly upon photolysis. *Proc. Natl. Acad. Sci. USA*. 91:187–191. http:// dx.doi.org/10.1073/pnas.91.1.187
- Harper, S.M., L.C. Neil, and K.H. Gardner. 2003. Structural basis of a phototropin light switch. Science. 301:1541–1544. http://dx.doi.org/10.1126/ science.1086810

- Harper, S.M., L.C. Neil, I.J. Day, P.J. Hore, and K.H. Gardner. 2004. Conformational changes in a photosensory LOV domain monitored by time-resolved NMR spectroscopy. J. Am. Chem. Soc. 126:3390–3391. http://dx.doi.org/10.1021/ja038224f
- Hirschberg, K., C.M. Miller, J. Ellenberg, J.F. Presley, E.D. Siggia, R.D. Phair, and J. Lippincott-Schwartz. 1998. Kinetic analysis of secretory protein traffic and characterization of golgi to plasma membrane transport intermediates in living cells. J. Cell Biol. 143:1485–1503. http://dx.doi.org/10.1083/jcb.143.6.1485
- Horton, A.C., and M.D. Ehlers. 2003a. Dual modes of endoplasmic reticulumto-Golgi transport in dendrites revealed by live-cell imaging. *J. Neurosci.* 23:6188–6199.
- Horton, A.C., and M.D. Ehlers. 2003b. Neuronal polarity and trafficking. *Neuron*. 40:277–295. http://dx.doi.org/10.1016/S0896-6273(03)00629-9
- Horton, A.C., B. Rácz, E.E. Monson, A.L. Lin, R.J. Weinberg, and M.D. Ehlers. 2005. Polarized secretory trafficking directs cargo for asymmetric dendrite growth and morphogenesis. *Neuron*. 48:757–771. http://dx.doi.org/ 10.1016/j.neuron.2005.11.005
- Inoue, T., W.D. Heo, J.S. Grimley, T.J. Wandless, and T. Meyer. 2005. An inducible translocation strategy to rapidly activate and inhibit small GTPase signaling pathways. *Nat. Methods*. 2:415–418. http://dx.doi.org/ 10.1038/meth763
- Jaiswal, J.K., V.M. Rivera, and S.M. Simon. 2009. Exocytosis of post-Golgi vesicles is regulated by components of the endocytic machinery. *Cell*. 137:1308–1319. http://dx.doi.org/10.1016/j.cell.2009.04.064
- Kaplan, J.H., and A.P. Somlyo. 1989. Flash photolysis of caged compounds: new tools for cellular physiology. *Trends Neurosci*. 12:54–59. http://dx.doi.org/10.1016/0166-2236(89)90136-7
- Kennedy, M.J., R.M. Hughes, L.A. Peteya, J.W. Schwartz, M.D. Ehlers, and C.L. Tucker. 2010. Rapid blue-light-mediated induction of protein interactions in living cells. *Nat. Methods*. 7:973–975. http://dx.doi.org/10 .1038/nmeth.1524
- Leivar, P., E. Monte, Y. Oka, T. Liu, C. Carle, A. Castillon, E. Huq, and P.H. Quail. 2008. Multiple phytochrome-interacting bHLH transcription factors repress premature seedling photomorphogenesis in darkness. *Curr. Biol.* 18:1815–1823. http://dx.doi.org/10.1016/j.cub.2008.10.058
- Levskaya, A., O.D. Weiner, W.A. Lim, and C.A. Voigt. 2009. Spatiotemporal control of cell signalling using a light-switchable protein interaction. *Nature*. 461:997–1001. http://dx.doi.org/10.1038/nature08446
- Liu, H., X. Yu, K. Li, J. Klejnot, H. Yang, D. Lisiero, and C. Lin. 2008. Photoexcited CRY2 interacts with CIB1 to regulate transcription and floral initiation in Arabidopsis. *Science*. 322:1535–1539. http://dx.doi.org/10.1126/science.1163927
- Lodish, H.F., and R.A. Weiss. 1979. Selective isolation of mutants of vesicular stomatitis virus defective in production of the viral glycoprotein. J. Virol. 30:177–189.
- Lungu, O.I., R.A. Hallett, E.J. Choi, M.J. Aiken, K.M. Hahn, and B. Kuhlman. 2012. Designing photoswitchable peptides using the AsLOV2 domain. *Chem. Biol.* 19:507–517. http://dx.doi.org/10.1016/j.chembiol.2012.02.006
- Ni, M., J.M. Tepperman, and P.H. Quail. 1998. PIF3, a phytochrome-interacting factor necessary for normal photoinduced signal transduction, is a novel basic helix-loop-helix protein. *Cell*. 95:657–667. http://dx.doi.org/10.1016/S0092-8674(00)81636-0
- Ni, M., J.M. Tepperman, and P.H. Quail. 1999. Binding of phytochrome B to its nuclear signalling partner PIF3 is reversibly induced by light. *Nature*. 400:781–784. http://dx.doi.org/10.1038/23500
- Nishimura, N., and W.E. Balch. 1997. A di-acidic signal required for selective export from the endoplasmic reticulum. *Science*. 277:556–558. http:// dx.doi.org/10.1126/science.277.5325.556
- Presley, J.F., N.B. Cole, T.A. Schroer, K. Hirschberg, K.J. Zaal, and J. Lippincott-Schwartz. 1997. ER-to-Golgi transport visualized in living cells. *Nature*. 389:81–85. http://dx.doi.org/10.1038/38891
- Rivera, V.M., X. Wang, S. Wardwell, N.L. Courage, A. Volchuk, T. Keenan, D.A. Holt, M. Gilman, L. Orci, F. Cerasoli Jr., et al. 2000. Regulation of protein secretion through controlled aggregation in the endoplasmic reticulum. *Science*. 287:826–830. http://dx.doi.org/10.1126/science.287.5454.826
- Rizzini, L., J.J. Favory, C. Cloix, D. Faggionato, A. O'Hara, E. Kaiserli, R. Baumeister, E. Schäfer, F. Nagy, G.I. Jenkins, and R. Ulm. 2011. Perception of UV-B by the Arabidopsis UVR8 protein. *Science*. 332:103–106. http://dx.doi.org/10.1126/science.1200660
- Rollins, C.T., V.M. Rivera, D.N. Woolfson, T. Keenan, M. Hatada, S.E. Adams, L.J. Andrade, D. Yaeger, M.R. van Schravendijk, D.A. Holt, et al. 2000. A ligand-reversible dimerization system for controlling protein-protein interactions. *Proc. Natl. Acad. Sci. USA*. 97:7096–7101. http://dx.doi.org/ 10.1073/pnas.100101997
- Schmoranzer, J., and S.M. Simon. 2003. Role of microtubules in fusion of post-Golgi vesicles to the plasma membrane. Mol. Biol. Cell. 14:1558–1569. http://dx.doi.org/10.1091/mbc.E02-08-0500

- Schmoranzer, J., M. Goulian, D. Axelrod, and S.M. Simon. 2000. Imaging constitutive exocytosis with total internal reflection fluorescence microscopy. J. Cell Biol. 149:23–32. http://dx.doi.org/10.1083/jcb.149.1.23
- Shimizu-Sato, S., E. Huq, J.M. Tepperman, and P.H. Quail. 2002. A light-switchable gene promoter system. *Nat. Biotechnol.* 20:1041–1044. http://dx.doi.org/10.1038/nbt734
- Strickland, D., K. Moffat, and T.R. Sosnick. 2008. Light-activated DNA binding in a designed allosteric protein. *Proc. Natl. Acad. Sci. USA*. 105:10709– 10714. http://dx.doi.org/10.1073/pnas.0709610105
- Strickland, D., Y. Lin, E. Wagner, C.M. Hope, J. Zayner, C. Antoniou, T.R. Sosnick, E.L. Weiss, and M. Glotzer. 2012. TULIPs: tunable, light-controlled interacting protein tags for cell biology. *Nat. Methods*. 9:379–384. http:// dx.doi.org/10.1038/nmeth.1904
- Toomre, D., J.A. Steyer, P. Keller, W. Almers, and K. Simons. 2000. Fusion of constitutive membrane traffic with the cell surface observed by evanescent wave microscopy. *J. Cell Biol.* 149:33–40. http://dx.doi.org/10.1083/jcb.149.1.33
- Tucker, C.L. 2012. Manipulating cellular processes using optical control of protein-protein interactions. *Prog. Brain Res.* 196:95–117. http://dx.doi.org/10.1016/B978-0-444-59426-6.00006-9
- Tyszkiewicz, A.B., and T.W. Muir. 2008. Activation of protein splicing with light in yeast. *Nat. Methods*. 5:303–305.
- Wu, D., Q. Hu, Z. Yan, W. Chen, C. Yan, X. Huang, J. Zhang, P. Yang, H. Deng, J. Wang, et al. 2012. Structural basis of ultraviolet-B perception by UVR8. Nature. 484:214–219. http://dx.doi.org/10.1038/nature10931
- Wu, Y.I., D. Frey, O.I. Lungu, A. Jaehrig, I. Schlichting, B. Kuhlman, and K.M. Hahn. 2009. A genetically encoded photoactivatable Rac controls the motility of living cells. *Nature*. 461:104–108. http://dx.doi.org/ 10.1038/nature08241
- Yazawa, M., A.M. Sadaghiani, B. Hsueh, and R.E. Dolmetsch. 2009. Induction of protein-protein interactions in live cells using light. *Nat. Biotechnol.* 27:941–945. http://dx.doi.org/10.1038/nbt.1569
- Zhang, M., H. Chang, Y. Zhang, J. Yu, L. Wu, W. Ji, J. Chen, B. Liu, J. Lu, Y. Liu, et al. 2012. Rational design of true monomeric and bright photoactivatable fluorescent proteins. *Nat. Methods*. 9:727–729. http://dx.doi.org/10.1038/nmeth.2021